Isotropic BRDF Measurements with Quantified Uncertainties

Ramon Hegedus, Antoine Lucat, Justine Redon, Romain Pacanowski

▶ **To cite this version:**

Isotropic BRDF Measurements with Quantified Uncertainties

R. Hegedus[1] and A. Lucat[2] and J. Redon[2] and R. Pacanowski[2]

[1] Department of Cognitive Neuroscience, Eberhard Karls University, Tubingen
[2] LP2N (CNRS) & Institut d'Optique Graduate School & INRIA

Abstract
Image-based BRDF measurements on spherical material samples present a great opportunity to shorten significantly the acquisition time with respect to more traditional, non-multiplexed measurement methods for isotropic BRDFs. However, it has never been analyzed deeply, what measurement accuracy can be achieved in such a setup; what are the main contributing uncertainty factors and how do they relate to calibration procedures. In this paper we present a new set of isotropic BRDF measurements with their radiometric and geometric uncertainties acquired within such an imaging setup. We discuss the most prominent optical phenomena that affect measurement accuracy and pave the way for more thorough uncertainty analysis in forthcoming image-based BRDF measurements. Our newly acquired data with their quantified uncertainties will be helpful for comparing the quality and accuracy of the different experimental setups and for designing other such image-based BRDF measurement devices.

Categories and Subject Descriptors (according to ACM CCS): I.3.3 [Computer Graphics]: Picture/Image Generation—BRDF Measurements Analysis

1. Motivation and Related Work

Since the seminal work of Marschner [Mar98] or Matusik et al. [MPBM03] on BRDF acquisition, a lot of devices and measurement setups have been developed to acquire the appearance of materials.

For the last two decades, most researchers from the Vision or CG communities have focused on acquiring acquire more complex appearance functions, such as spatially-varying BRDF (e.g., [McA02, LBAD*06]) to Bidirectional Texture function (e.g., [DvGNK99]) or tried to reduce setups complexity or cost (e.g., [RWS*11]). Unfortunately, most setups or available measurements data are hard to compare because they rely on qualitative validation instead of a quantitative one. For example, many papers (e.g., [NDM05]) that try to fit BRDF analytical models discard measurements at arbitrary grazing angles because they «seem» unreliable.

We believe that new available data with their quantified uncertainties will be helpful for the research community, especially in order to compare the quality and accuracy of the different experimental setups and even to help other research teams to develop their devices. Furthermore, uncertainty values can be useful to guide approximation techniques (e.g., Levenberg-Marquardt, SQP, Weighted Least-Square),which are necessary to obtain parameters of analytical models.

This paper presents a **new set of isotropic BRDF measurements with their radiometric and geometric uncertainties** acquired from our imaging device (cf. Section 2). The uncertainties are derived from a model (cf. Section 3) that take into account different source of errors (e.g., focal length, mechanical, ...). In section 4 we illustrate through various plots the different uncertainties obtained with our setup and also illustrate the acquired BRDFs. Finally, we discuss the limitations of our current uncertainty model and offer possible improvements for it.

2. BRDF Setup

Our setup shares similarities from the one introduced by Matusik et al.. As shown in Figure 1 in our setup we measure the BRDF of materials on a spherical sample by acquiring multiple images using a Jenoptik scientific camera (ProgRes C14 Plus). The camera is firmly mounted on an arm that is fixed to a rotation stage (from Zaber T-RS60). The material sample (i.e., a target sphere of approx. 6cm) is placed on a support also fixed to the rotating arm. Contrary to previous setups, our light source is a fixed collimated beam that lits the entire target sphere. In another words the camera and the target sphere are always facing each other, regardless of the rotation step. However, they are moving wrt. to the light source thanks to the rotating arm, which makes possible to
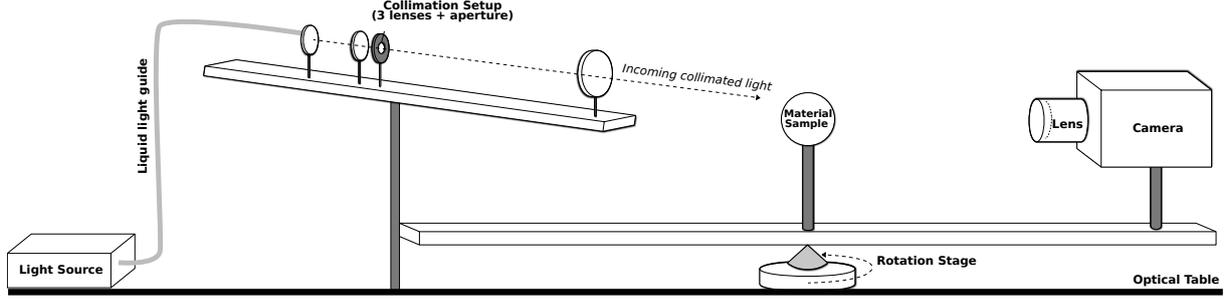
Figure 1: *Schematic view of our acquisition setup.*

have the three degrees of freedom required to measure an isotropic BRDF.

The goal of our setup is to measure a spatially uniform isotropic BRDF. As defined by Nicodemus [NRH*77], the BRDF f_r is a positive quantity expressed in sr^{-1} (inverse steradian) representing how a material reflects *angularly* the light. For a given point p_S on a surface S f_r is defined as the ratio of the differential reflected radiance L_r and the differential irradiance dE:

$$f_r(\theta_i, \theta_o, \Delta_\phi) = \frac{L_r(\theta_o, \phi_o)}{dE(\theta_i, \phi_i)}$$

where all angles $(\theta_i, \theta_o, \Delta_\phi = |\phi_o - \phi_i|)$ are expressed in the local (tangent) frame of the surface orientated with a normal vector $\mathbf{n}_s$. When using a broadband white light source with an RGB-sensor, the measured BRDF can be seen as an angular function returning an RGB HDR value:

$$f_r(\theta_i, \theta_o, \Delta_\phi) \rightarrow (\rho_r, \rho_g, \rho_b). \qquad (1)$$

The geometric calibration step is responsible to establishing the angular values $(\theta_i, \theta_o, \Delta_\phi)$, whereas the radiometric calibration is necessary for the BRDF values themselves.

Geometric Calibration As in Matusik et al. setup, the fact to have a fixed camera with respect to the target sphere presents the advantage to calibrate (geometrically) the camera only once. Calibrating the camera is done using the Caltech library [Bou] with the associated thin-lens model. This model is also able to take into account distortion, but the calibration process did not compute meaningful values for our camera and therefore we simply discarded these parameters. The camera calibration allows us to recover the per-pixel view direction as well as the focal length.

The second calibration step is to recover the target sphere position in the camera frame, assuming its radius is known (e.g., provided by the manufacturer). This can be done easily by noticing that a perspective projection of a sphere provides a perfect elliptical contour. Fitting this ellipse directly gives the sphere center, with a very good accuracy.

Finally, in order to recover the light direction (in camera

$f_r(\theta_i, \theta_o, \Delta_\phi)$	Isotropic BRDF function
ρ_r, ρ_g, ρ_b	BRDF RGB values
S	Sphere on which the BRDF is measured
$\theta_i, \theta_o, \Delta\phi$	Angles in the tangent frame of S
p_S	Point on S
$\mathbf{n}_s$	Normal vector of p_S
$(r_s, \mathbf{c}_s)$	Radius and position of the sphere
$\mathbf{A}$	Rotation axis of the illumination vector
F	Focal length
$\mathbf{o}$	Optical axis of the camera
p_{ccd}	Pixel on the sensor
s_{ccd}	Size of a pixel ($6.45 \times 6.45 \text{microns}^2$)
$E_{r,g,b}(p_{ccd})$	HDR Values (Irradiance) at p_{ccd}
ω_o	Camera view vector in camera space
ϕ_{stage}	Angle of the rotation stage
$U(\mathbf{x})$	Uncertainty function

Figure 2: *Mathematical notations used in this paper. Please refer to Figure 4 to see how these quantities relate to each other in terms of uncertainties.*

space), we use a mirror sphere as target and record multiple images of the specular highlight visible on the sphere. By assuming a perfect mirror, we compute the reflected ray impacting from the light spot for various camera-light configurations. This process gives a 3D locus of the light direction, which can be accurately described by a rotation axis and a latitude.

We deduce from the camera calibration and the radius of the target sphere its position wrt. to the camera. Then, we ray-trace a virtual sphere in order to estimate the normal vector in each pixel. Finally, combining the light direction, the view vectors and the per-pixel normal vectors we get an estimate, per pixel, of the three angles $(\theta_i, \theta_o, \Delta\phi)$ of an isotropic BRDF measurement.

Radiometric Calibration We analyzed the radiometric response of our camera, which is an important factor to consider in order that accurate radiance values be measured.
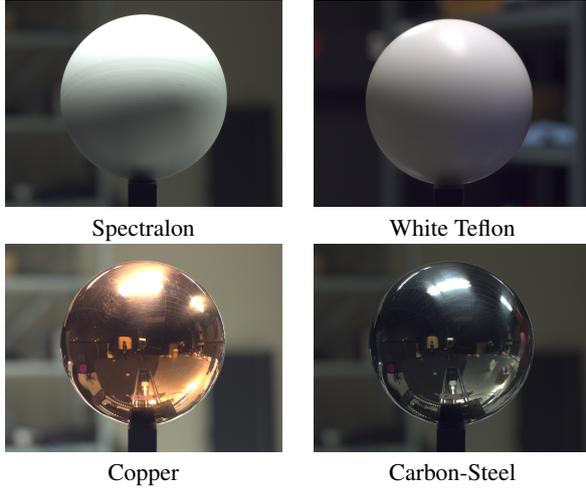
Spectralon

White Teflon

Copper

Carbon-Steel

Figure 3: *The four materials measured for this paper.*

Since our setup accommodates a stabilized light source and the camera has an electronic shutter that allows for precise exposure time control, we have chosen a simple, yet efficient way of acquiring the response curve. The light was directed towards the camera lens, in front of which a thin diffuser sheet was fixed, thus the same image of the diffused source light was recorded multiple times with different exposure times. Then the median pixel value in each of R,G,B channels throughout the whole image was selected. In this way median value vs. exposure time directly yields the response curve, since exposure time is directly proportional to incoming total radiance. These data showed that radiometric response is totally linear as long as pixel value, encoded with 14 bits, is less than 15800 (values over 15800 were simply discarded). The other common correction related to color measurements is to make RGB values independent from the sensor spectral sensor sensitivity and the spectral light composition. This correction procedure can be done using a reference object, in our case a spherical Spectralon that is designed precisely to have a uniform spectral reflectance. Imaging this object allows to find the correct multiplicative factors to apply on each color channel in order to recover correct relative (inter-color-channel) values.

Material Samples As shown in Figure 3, we acquired four materials ranging from a very diffuse (Spectralon) to an almost perfect mirror sphere made of carbon-steel. We used the carbon-steel ball as reference for the radius, since the manufacturer provides its radius (6cm) with a 50 μm uncertainty. For the other material samples, we compute the radius using the carbon steel sphere as a reference. If we replace it by another sphere of unknown radius, we can recover its position and radius by the ellipse fitting method previously described, knowing the depth in the camera frame instead of the radius. We assumed bilateral symmetry (i.e., symmetry

of the BRDF wrt. to the incident plane) of an isotropic BRDF and therefore our setup acquired 221 images (1360x1024 pixels) by moving the rotation arm 0.75 degrees in each step. This resolution gives about 60 million samples for each measured material. More precise measurements can be achieved by reducing the rotation step of the stage (up to. 0.0002 degree). However, it is important to keep in mind that the angular resolution of the BRDF measurement also depends on the camera sensor resolution, as it ranges from 0.1° resolution for a normal viewing direction to 2° at 50° and reaches 12° for grazing angles. θ_i is ranging from 0 to 90°, θ_o from 0 to 85°, $\Delta\phi$ from 0 to 180°. Finally, all material measurements will be released on the ALTA [BCP*15] project website.

3. Uncertainty Model

In this paper we are interested in establishing the uncertainties σ associated with the BRDF values $(\sigma_{\rho_r}, \sigma_{\rho_b}, \sigma_{\rho_b})$ as well as with the geometrical positions of the measurements $(\sigma_{\theta_o}, \sigma_{\theta_i}, \sigma_{\Delta\phi})$. Figure 4 shows how the uncertainties of a BRDF measurement are related to the calibration parameters of the different parts of the setup. Some uncertainties such as the radius of the sphere or the pixel size are directly given by manufacturers. Radii of the spheres were given up to $50\mu m$, whereas the pixel size is known up to $0.005\mu m$. For the mechanical uncertainty of the rotation stage we verified that the repeatability and uncertainty numbers given by the manufacturer were correct. In order to increase the precision of the measurement, the stage is always set to rotate only by a discreet number of steps. All other uncertainties are derived from either radiometric or geometric calibration procedure. More formally, the uncertainties σ of a given parameter is a function of the following parameters:

$$\sigma_{\theta_i, \Delta\phi} = U(F, s_{ccd}, r_s, \mathbf{c}_s, \alpha, \mathbf{A}, \phi_{\text{stage}}) \quad (2)$$

$$\sigma_{\theta_o} = U(F, s_{ccd}, r_s, \mathbf{c}_s) \quad (3)$$

$$\sigma_{\rho_r, \rho_g, \rho_b} = U(E_{r,g,b}(p_{ccd}), \omega_o, F, \theta_i) \quad (4)$$

Instead of deriving an analytical formula we choose to numerically compute the partial derivatives of U for each parameter. For our setup we obtain the following uncertainties: the focal length of the camera uncertainty is $\sigma_F = 0.3360mm$ and the sphere position $\sigma_{\vec{c}_s} = (0.0051225, 0.0026681, 4.879)\,mm$.

When considering a uniform transmitting lens, a uniform illumination light-field, and neglecting convolution effects (diffraction, aberrations, and light divergence), one can show that the BRDF is governed to the irradiance on the sensor by the following equation:

$$f_r(\theta_o, \theta_i, \Delta\phi) = K \frac{E_{r,g,b}(p_{ccd}) F^2}{\cos\theta_i (\cos\theta_o)^4} \quad (5)$$

where K is scaling factor that can be determined by using a known target such as our Spectralon. Therefore, the radiometric related uncertainties $\sigma_{\rho_r, \rho_g, \rho_b}$ depend on the HDR values, for which the main source of error is due to photon
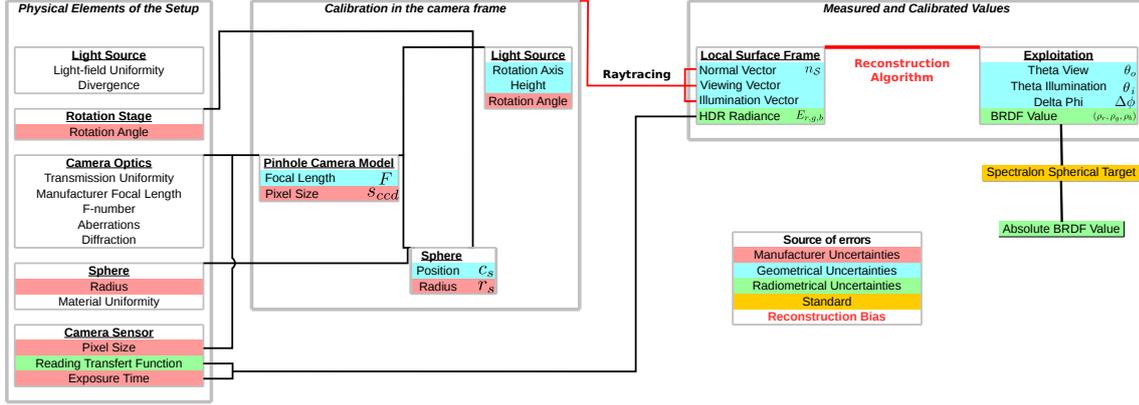
Figure 4: *Relationship and connection of the different uncertainties. The different colors illustrate the source of errors that are taken into account in our uncertainty model. The full analytical formula that relates every setup parameter to the BRDF value is in reality more complex and, particularly, non-invertible. For this reason, we have to use an algorithm that gives an approximate result of the measurement, in our case, the zero-order approximation (equation 5). Much complex approximations would lead to more accurate BRDF values, but we will always have to consider a reconstruction bias.*
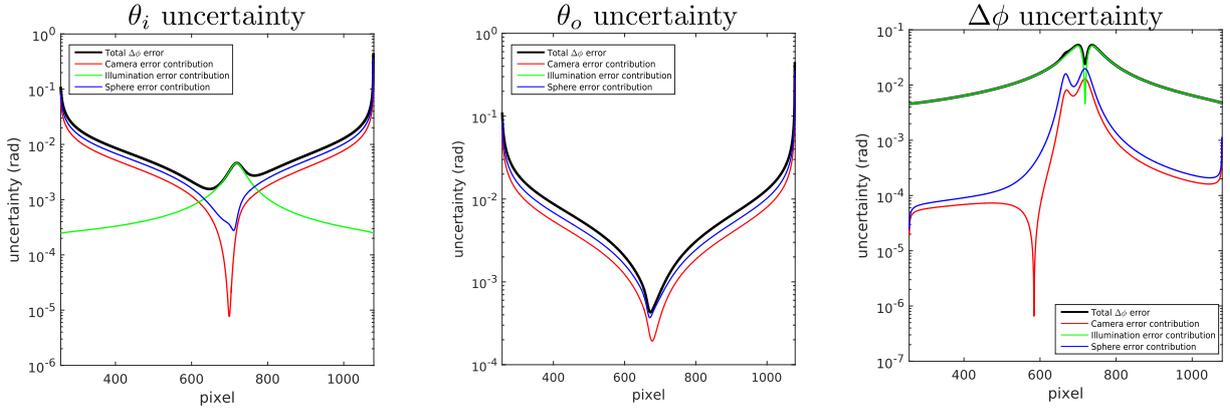

Figure 5: *Uncertainty values for the BRDF angles $(\theta_i, \theta_o, \Delta\phi)$ when $\phi_{stage} = 7°$.*

shot noise as well as other sources such as the square of the focal length, the cosine factor $\cos\theta_i$ the vignetting effect (or fall-off) $(\cos\theta_o)^4$. For our setup the fall-off factor is very low since its maximum value is 0.9957 at the silhouette of the sphere (compared to 1.0 at the center). Figures 5 presents the uncertainties values related to the geometrical calibration. As one could expect, geometrical calibrated values become less and less reliable (up to 4 order of magnitude) when approaching grazing angle. The full analytical formula that relates every setup parameter to the BRDF value is in reality more complex and, particularly, non-invertible. For this reason, we have to use an algorithm that gives an approximate result of the measurement, in our case (equation 5), the zero-order approximation.

4. Measurements Results

Figure 6 presents the BRDF measurements in the incident plane with uncertainties for the different material samples. Figure 7 shows the measured values of BRDF for Teflon material in 2D polar plot. Overall, the error on the BRDF values varies from 3% at normal incidence to 5% at 50° and reaches 30% at 85°

5. Discussion

The presented measurements with their uncertainties are primarily valid for our precise setup. Because of the complex interrelations among uncertainties of various parameters pertaining to such measurements, some general conclusions can be hard to find, nevertheless some hints can be deduced from our study. Below we discuss three important optical effects
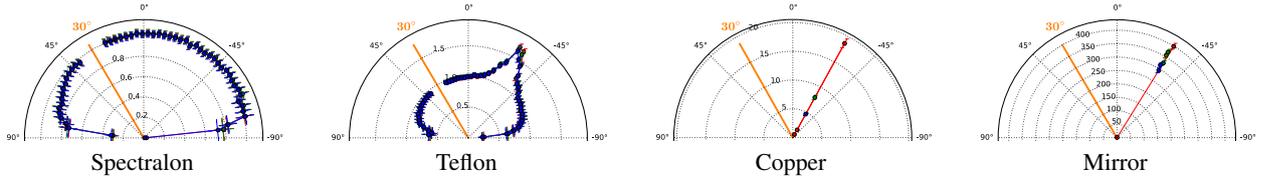
Figure 6: *Incident plane BRDF measurements with uncertainty bars for the four materials.*
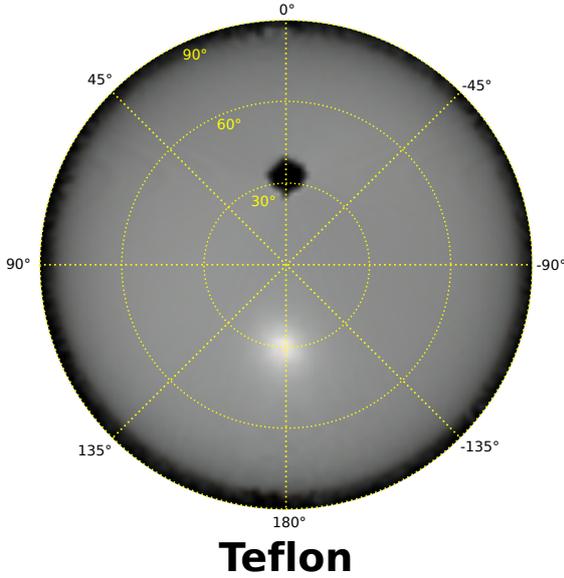

Figure 7: *BRDF values for the Teflon material for $\theta_i = 30°$*

that arise when measuring physical quantities with imaging system.

Diffraction from the Camera Aperture An important optical factor that needs proper attention in a camera-based BRDF acquisition setup, and is often overlooked, is diffraction originating from the aperture of the camera. The more stopped-down is the aperture the more diffraction will arise. Since we use a well stopped down aperture (f/8) in the camera lens and with good reason the effect cannot be neglected. Although opening the aperture would practically eliminate problems caused by diffraction, it is not a good idea, because then lens aberrations would quickly become dominant and depth of field (which is needed for spherical samples) would also reduce, causing inaccuracies of an other nature that are actually more difficult to handle. The main effects of diffraction on the accuracy of obtained BRDF values are twofold (although in reality they arise from the same, single physical effect causing a convolution in the image). Firstly, there is a general blurring effect that can be modeled by taking into account the first order of a circular Airy disk pattern as

convolution kernel. The second effect, is the so-called starburst effect on highlights, the cause of which is that light gets diffracted through the aperture (hexagonal blades in our setup). In our experience the general blurring effect in our setup is negligible compared to other convolution-type effects (depth of field confusion, imperfect collimation of the light source, and surface roughness), and that is for this reason that we set the aperture to a large value (f/8). However, the star-burst pattern around highlights is very much apparent and practically unavoidable. This forces us to drastically reduce the time of exposure range of the HDR imaging, and consequently the dynamic range of the BRDF measurement. In reality, the sharper the highlights on the material surface the stronger this effect. Thus, in the worst-case scenario of BRDF with a very specular component, we can only reach a 20× factor between the shortest and the longest time of exposure. The more diffuse the material, the higher this factor, so that this restriction is eased. In this work, we have not addressed this problem yet and we simply stop recording data when the effect arises.

Diffraction White Light Speckle Another last effect of the diffraction is due to the surface roughness, it is generally known as the white light speckle [McK76]. It arises from the fact that on a small enough surface the light becomes coherent and produces grating-like light pattern when bouncing off a rough surface. If the surface is smooth or rough enough, this effect disappears but in between it becomes prominent. For incident light angles up to 60°, the main effect is changing locally color of the reflected light, and for more grazing angles, it also introduces a shift in the reflection angles (similarly to the effect of a grating). It then falsifies the material spatial uniformity and introduces a structured color noise. A major consequence is that, in reality, this coherence disappears with the divergence of the incoming light (as is the case in usual daily life when observing a scene), so using BRDF data from such a measurement introduces a perception bias, which can be inconvenient for a rendering purpose.

Out-of focus effect of common lenses One common issue with lenses is their lack of large depth of field, which introduces an error when measuring the BRDF with an imaging system. Indeed, one pixel of the CCD sensor recovers an irradiance value that is the convolution of the illumination with a portion (and not only a single point p_S) of the sphere and the BRDF. Deriving the uncertainty is a complex
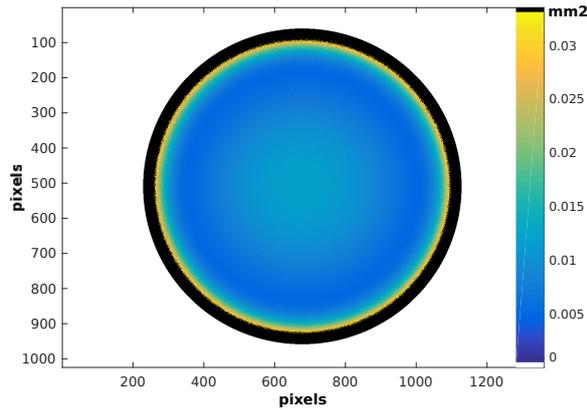
Figure 8: *Illustration of the out-of-focus effect when imaging a sphere. The picture shows for each pixel of the acquired image how much the optical rays from the lens camera cover the target sphere. The larger this spread the larger the error on the BRDF measurement. The spread is minimal only for the part of the target sphere which is at perfect focus. For our setup, the sphere radius is 6cm and the focus is made at 4.2cm from the sphere center (corresponding to an in-focus plane at $45°$ latitude). The black area starts at $\theta_o = 68°$ and finishes at $\theta_o = 85°$ where the maximum area is about $2.1mm^2$.*

task that we did not take into account in this paper. However, we simulated precisely how large the different areas on the sphere are, across which the convolution applies. As shown in Figure 8 the area size ranges from $0.001mm^2$ (part of the sphere which are in focus) to $2.1mm^2$ (grazing angles). Note that we set the focus distance at $45°$ latitude as a compromise.

6. Future Work

As future work we would like to improve our uncertainty model by taking into account the potential (spatial and directional) non-uniformity of the light source, or the lens and also remove on-the-fly pixels where the aperture diffraction appears. Furthermore, we would also like to average temporally our measurements to avoid white light speckle effects.We would also like to take into account correlation between the different uncertainties by computing numerically the co-variance matrix of the different factors. Furthermore, we would also like to study how the different BRDF models approximate these data with respect to the uncertainties provided. Finally, we will also provide additional measurements for other materials to improve our qualified database.

References

[BCP*15] BELCOUR L., COURTES L., PACANOWSKI R., ET AL.: ALTA: A BRDF Analysis Library. http://alta.gforge.inria.fr/, 2013-2015. 3

[Bou] BOUGUET J.-Y.: Camera calibration toolbox. URL: http://www.vision.caltech.edu/bouguetj/calib_doc/. 2

[DvGNK99] DANA K. J., VAN GINNEKEN B., NAYAR S. K., KOENDERINK J. J.: Reflectance and texture of real-world surfaces. *ACM Trans. Graph. 18*, 1 (Jan. 1999), 1–34. 1

[LBAD*06] LAWRENCE J., BEN-ARTZI A., DECORO C., MATUSIK W., PFISTER H., RAMAMOORTHI R., RUSINKIEWICZ S.: Inverse shade trees for non-parametric material representation and editing. In *Proc. ACM SIGGRAPH '06* (2006), pp. 735–745. 1

[Mar98] MARSCHNER S. R.: *Inverse rendering for computer graphics*. PhD thesis, 1998. 1

[McA02] MCALLISTER D.: *A generalized Representation of Surface Appearance*. PhD thesis, University of North Carolina at Chapel Hill, 2002. 1

[McK76] MCKECHNIE T. S.: Image-plane speckle in partially coherent illumination. *Optical and Quantum Electronics 8*, 1 (1976), 61–67. 5

[MPBM03] MATUSIK W., PFISTER H., BRAND M., MCMILLAN L.: Efficient isotropic BRDF measurement. In *Proc. EGWR '03* (2003), pp. 241–247. 1

[NDM05] NGAN A., DURAND F., MATUSIK W.: Experimental analysis of BRDF models. In *Proc. EGSR '05* (2005), pp. 117–226. 1

[NRH*77] NICODEMUS F., RICHMOND J., HSIA J., GINSBERG I., LIMPERIS T.: *Geometrical Considerations and Nomenclature for Reflectance*. 1977. 2

[RWS*11] REN P., WANG J., SNYDER J., TONG X., GUO B.: Pocket reflectometry. *ACM Trans. Graph. 30*, 4 (July 2011), 45:1–45:10. 1